On cavitation occurrence in perforated plates

Stefano Malavasi [a], Gianandrea Vittorio Messa [a,*], Umberto Fratino [b], Alessandro Pagano [b]

[a] *DICA, Politecnico di Milano, Piazza Leonardo da Vinci, 32–20133 Milano, Italy*
[b] *DICATECh, Politecnico di Bari, Via Orabona, 4–70125 Bari, Italy*

1. Introduction

Perforated plates are normally used within pressurized systems, as control or maintenance devices. Generally, these devices are installed upstream flowmeters for removing swirl and correcting a distorted flow profile or, coupled with a control valve, for preventing cavitation phenomena, assuring safe operating conditions [1,2].

Studies about the hydraulics of perforated plates are rather abundant; some of them aim at investigating the functionality of these devices as flow conditioners [3–7], being focused on their use for pre-conditioning a disturbed flow, whereas others mainly concern the analysis on the dissipation characteristics of perforated plates [8–18]. On the contrary, studies on the cavitation behavior of perforated plates are relatively few, despite the topic is engineering relevant. Most of the investigations concerning cavitation phenomena consider single hole plates [1,2,19–32], whilst the multi-hole case was addressed very rarely [33–35]. At present, the most comprehensive investigations about this topic seem those from Maynes and his co-workers [15,18], who analyzed the effect of the plate geometry on its cavitation characteristics; this research was anticipated by a preliminary work of one of the authors of the present article [36]. The present work fits into this context and aims at carrying forward the above-mentioned investigations, particularly providing further information related to cavitation inception in differently shaped perforated plates.

Cavitation can be roughly considered as the rapid vaporization and condensation of a liquid, caused by a sudden pressure reduction [37]. According to the ISA standard [38], different cavitation regimes can be identified measuring the indirect effects induced by cavitation phenomena in a hydraulic system, as the vibration: 1) REGIME I: absence of cavitation; 2) REGIME II: incipient cavitation, namely the onset of cavitation, where only small vapor bubbles are formed in the flow stream. This condition is detected when an abrupt increase in induced vibration level occurs after the collapse of the bubbles and the condensation of the vapor; 3) REGIME III: constant cavitation, involving a sufficiently large volume of vapor to produce a uniform and constant level of cavitation; 4) REGIME IV: maximum vibration, that is, the level of cavitation associated with occurrence of choking condition. The level of cavitation causing damages to a device is hard to define and is usually indicated on the basis of experience. Clearly the more conservative choice consists of restricting all operations to a cavitation-free regime even if typically the incipient cavitation level (REGIME II) may be acceptable in the design phase [1,38].

Cavitation is usually studied by means of the cavitation number for which several definitions exist. Hereafter, the following cavitation parameter definition, as proposed by the ISA standard [38], will be used:

$$\sigma = \frac{P_1 - P_V}{P_1 - P_2} \tag{1}$$

where P_1 and P_2 are the pressures measured sufficiently far upstream and downstream the device (Fig. 1), in order to provide

* Corresponding author. Tel.: +39 02 2399 6287; fax: +39 02 2399 6298.
E-mail address: gianandreavittorio.messa@polimi.it (G.V. Messa).

A'	Acceleration (ms^{-2})
c'	Parameter in Eq. (8) (-)
C_c	Contraction coefficient (-)
C_d	Discharge coefficient (-)
d_h	Diameter of the holes (m)
D	Pipe diameter (m)
D_{ref}	Reference pipe diameter (m)
Eu	Euler number (-)
n_h	Number of holes (-)
P_1	Pressure at upstream reference section (Pa)
P_2	Pressure at downstream reference section (Pa)
P_V	Vapor pressure (Pa)
Re_h	Hole Reynolds number (-)
SSE	Size Scale Effects correction factor (-)
t	Plate thickness (m)
$u(\zeta)$	Absolute uncertainty on variable ζ
V	Pipe bulk-mean velocity (ms^{-1})
V_h	Average fluid velocity within the holes (ms^{-1})
Y	Parameter in Eq. (12) (-)
β	Equivalent diameter ratio (-)
$\varepsilon(\zeta)$	Relative uncertainty on variable ζ (-)
ν	Kinematic viscosity coefficient of the fluid $(\mathrm{m^2 s^{-1}})$
ρ	Fluid density (kgm^{-3})
σ	Cavitation number (-)
σ_2	Alternative definition of the cavitation number (-)
σ_c	Constant cavitation number (-)
σ_i	Incipient cavitation number (-)
σ_{mv}	Maximum vibration cavitation number (-)
σ_V	Alternative definition of the cavitation number (-)
MH	Multi-hole orifice
SH	Single-hole orifice
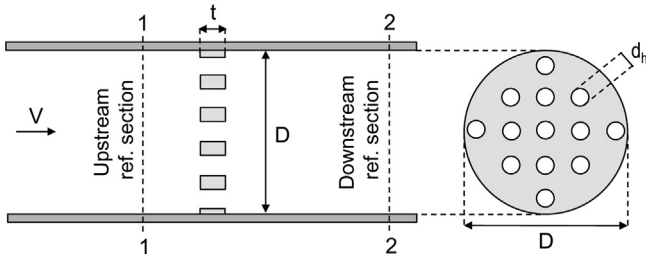
Fig. 1. Test longitudinal section: pressure measuring points.

Fig. 2. Identification of the cavitation regimes and limits according to the ISA standard [38].

reliable values of the gross pressure drop, and P_V is the vapor pressure. Similar definitions of the cavitation number, related to the above mentioned ones, are:

$$\sigma_2 = \frac{P_2 - P_V}{P_1 - P_2} = \sigma - 1 \qquad (2)$$

$$\sigma_V = \frac{P_1 - P_V}{1/2\rho V^2} = Eu \cdot \sigma \qquad (3)$$

where ρ is the fluid density, V is the pipe bulk-mean velocity (Fig. 1), and

$$Eu = \frac{P_1 - P_2}{1/2\rho V^2} \qquad (4)$$

is the Euler number.

Different threshold values of σ are defined: the incipient cavitation number σ_i, where Regime II starts; the constant cavitation number σ_c, where Regime II meets Regime III; and the maximum vibration cavitation number σ_{mv} where Regime III ends. The incipient cavitation number σ_i identifies the first detectable onset of cavitation and, according to the ISA standard [38], it can be experimentally estimated in a semi-log plot of acceleration or sound pressure level measurements versus the cavitation index σ, where a first sudden increase of the data trend occurs (Fig. 2). It's worth emphasizing the difficulties inherent in this graphical procedure, which make it difficult to accurately estimate σ_i.

The incipient cavitation number is likely to be affected by the geometrical characteristics of the devices, expressed by the following parameters: (1) the porosity of the screen, that is, the ratio of the open area to the overall pipe section, usually expressed using the equivalent diameter ratio β; (2) the plate thickness t, usually taken into account by means of the dimensionless relative thickness t/d_h, d_h being the hole diameter; (3) the number of holes n_h; (4) the
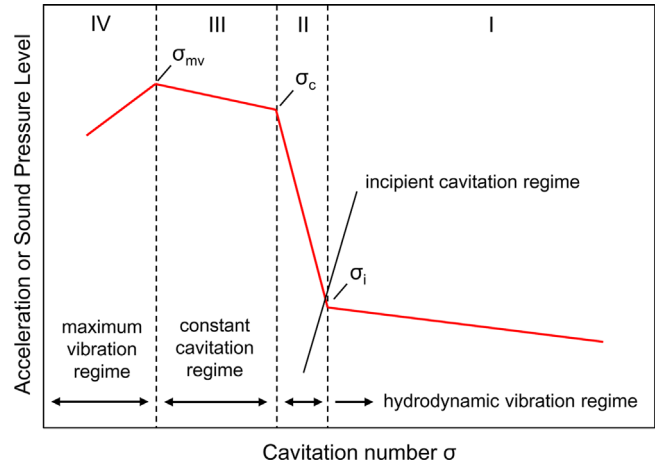
distribution of the holes and their shape, as well as the chamfering of their edges. In this article only devices having circular holes of uniform size, with a negligible radius of curvature at the edges of the holes, are considered. Although its influence is not analyzed in the present work, we underline that the shape of the holes is a key factor since the chamfering of the edges may result in a significant variation of the incipient cavitation number.

Holt et al. [15] found that the incipient cavitation number of perforated plates increases with β for $0.32 \leq \beta \leq 0.66$, meaning that cavitation inception is more likely to occur in plates with higher porosity. This result confirmed the outcomes of different researches regarding the single-hole case [1,2,20,21,23]. Nevertheless the effect of the relative thickness t/d_h on σ_i does not appear completely clarified yet. Maynes et al. [18] found that the trend of σ_i as a function of t/d_h is increasing until $t/d_h \approx 1$, and decreasing for longer orifices. The authors related this behavior to the transition within the holes between separated and reattached flows. Indeed, the dependence of σ_i upon n_h, the other parameters being the same, has never been systematically studied, as well as the influence of the shape, distribution, and chamfering of the holes.

Different approaches can be used for estimating the incipient cavitation number of perforated plates. In particular, two physically based models have been proposed by Nurick [24] and Sanchez et al.

[31]; in both of them, the discharge coefficient C_d, as defined by Eq. (5), appears among the independent variables:

$$C_d = \frac{V}{\sqrt{2(P_1 - P_2)/\rho + V^2}} = \frac{1}{\sqrt{Eu + 1}} \tag{5}$$

From Eq. (5) it is evident that C_d preserves the same functional dependencies as Eu, which proved to be affected by the equivalent diameter ratio β, the relative thickness t/d_h, the number n_h and the disposition of the holes, and the hole Reynolds number $Re_h = V_h d_h/\nu$ [17], where V_h is the average fluid velocity within the holes and ν is the kinematic viscosity coefficient of the fluid. However, it is well known [17,18] that the Euler number (and, consequently, the discharge coefficient) of perforated plates remains essentially constant within a certain range of Re_h.

Rearranging the model by Nurick [24], the incipient cavitation number of single-hole orifices with $0.08 \le \beta \le 0.39$ and $2 \le t/d_h \le 20$ can be estimated as follows:

$$\sigma_i = \frac{C_d^2}{1 - C_d^2} \frac{1}{\beta^4 C_c^2} \tag{6}$$

where C_c is the contraction coefficient of the jet, which the same author suggests to evaluate by means of the following empirical expression:

$$C_c = 0.62 + 0.38\beta^6 \tag{7}$$

Nurick [24] states that Eq. (6) could be used to determine the onset of cavitation, even if he never refers to "incipient cavitation number" in his paper. Eq. (6) was obtained by applying the Bernoulli equation for ideal flow between a section just upstream the orifice (assuming $V \approx 0$) and the vena contracta section, and imposing the pressure at the vena contracta to be equal to the vapor pressure. Since it is well known that the initiation of fluid cavitation occurs when the cavity pressure is well above the vapor pressure, we expect that Eq. (6) holds for higher cavitation levels, and therefore it will underestimate σ_i. The experiments of Nurick [24] seem to confirm that Eq. (6) provides reliable predictions of the cavitation number at choking cavitation as it is also mentioned in Testud et al. [35].

Starting from these considerations, Sanchez and co-workers [31] proposed an extension of Nurick's model, as follows:

$$\sigma_i = \frac{C_d^2}{1 - C_d^2} \left(\frac{1}{\beta^4 C_c^2} - 1 \right)(1 + c') + c' \tag{8}$$

where c' indicates the amplitude of the pressure fluctuations with respect to the velocity head at the vena contracta section. They found that the empirical correlation $c' = 2.9(D[m])^{0.5}$ procures quite good agreement with the incipient cavitation number estimates by Tullis [22]. Even if Eq. (8) was derived for single-hole orifices, Sanchez et al. [31] mention the possibility of applying this formula to other devices such as valves, if a suitable correlation for c' is provided.

Three empirical correlations for σ_i have been proposed based on best-fitting of experimental measurements. All models consist of polynomial equations which differ in the set of related parameters. The formula proposed by Kuroda et al. [25] expresses σ_i as a function of the equivalent diameter ratio β only and it can be applied to single-hole orifices with $0.2 \le \beta \le 0.6$:

$$\sigma_i = 1.5 + 4.5\beta \tag{9}$$

The correlation of Tullis, first proposed in [1] and later revised in [2], relates σ_i to the discharge coefficient C_d and it was obtained from the experimental data collected on five single-hole orifices with $0.39 \le \beta \le 0.80$ and $t/d_h \approx 0$ $(0.1 \le C_d \le 0.64)$. The latest formula is:

$$\sigma_i = 1.55 + 4.88 \cdot C_d + 5.66 \cdot C_d^2 + 1.85 \cdot C_d^3 \tag{10}$$

More recently, Maynes et al. [18] developed an empirical equation in which C_d is the independent variable, whilst the dependent one is a function of σ_i and t/d_h. This formula, obtained by fitting original experimental data using perforated plates with $0.33 \le \beta \le 0.67$, $0.24 \le t/d_h \le 3.38$, and $7 \le n_h \le 1793$ and Tullis' measurements [1] regarding single-hole orifices, reads as follows:

$$\frac{\sigma_i - 1}{1 - 0.1\frac{t}{d_h}} = 50.2 \cdot C_d^3 - 53.1 \cdot C_d^2 + 25.5 \cdot C_d - 0.31 \tag{11}$$

and the overall range of C_d spanned by these authors is $0.076 \le C_d \le 0.648$.

Pressure and size scale effects should also be carefully considered when investigating the cavitation in the hydraulic devices. The former effect consists in the possible influence of the operating pressure on the cavitation limits. Anyway, several researchers agreed that there are no pressure scale effects associated with incipient cavitation in case of perforated plates [1,21,23,33]. This was confirmed by our own experiments, as it will be discussed later in the article. Conversely, extensive research demonstrated that size scale effects are not negligible, with σ_i increasing with the pipe diameter [1,2,15,21,23,33]. The following adjustment was proposed by Rahmeyer [39] to account for size scale effects:

$$SSE = \left(\frac{D}{D_{ref}} \right)^Y \quad Y = 0.3Eu^{-0.25} \tag{12}$$

in which D_{ref} is a reference pipe diameter. Even if Rahmeyer [39] obtained Eq. (12) by fitting experimental data regarding several types of valves up to 0.915 m (36 in) diameter, Tullis [1] has confirmed its applicability to single-hole orifices as well.

Aim of this work is to investigate the cavitation behavior of perforated plates, with special regard to cavitation inception. For this purpose, a large database of experimental data is provided by joining the results of a wide experimental campaign performed on two separate and independent test rigs with data coming from technical literature, after having checked them for consistency and made comparable to ours. Such a database is aimed at different objectives. Firstly, the most significant parameters affecting the onset of cavitation are identified and their role analyzed. Secondly, starting from the correlations available in the literature, a set of dependent and independent parameters resulting in a satisfactory fitting of all the available data is identified. Finally, a new correlation is proposed for estimating the incipient cavitation number.

2. Test rigs and experimental procedure

Several tests were carried out by the research groups of Politecnico di Bari University and Politecnico di Milano University, using two different test rigs whose main features are summarized in the following, along with the testing procedure adopted in both campaigns.

Experimental activities were performed in a test rig located at the hydraulic laboratory of Politecnico di Bari University (Fig. 3). The system is supplied from a pump capable to guarantee pressures up to 2 bar upstream the plate and flow rates up to 110 l/s. The pump is located on a 203 mm (8 in) nominal diameter pipe, connected to the testing line, which has a nominal diameter of 50.8 mm (2 in) and an actual diameter of 53 mm. More than 5 m of straight pipes were left upstream the plate in order to guarantee that fully-developed flow conditions can be achieved. An equal length of straight pipe downstream the plate is more than enough to allow a complete pressure recovery. A couple of control valves placed upstream and downstream the testing line allowed the setting of the proper fluid-dynamic conditions for each experimental test. The pressure taps for evaluating the gross pressure drop were located 1D upstream and 10D downstream the device,
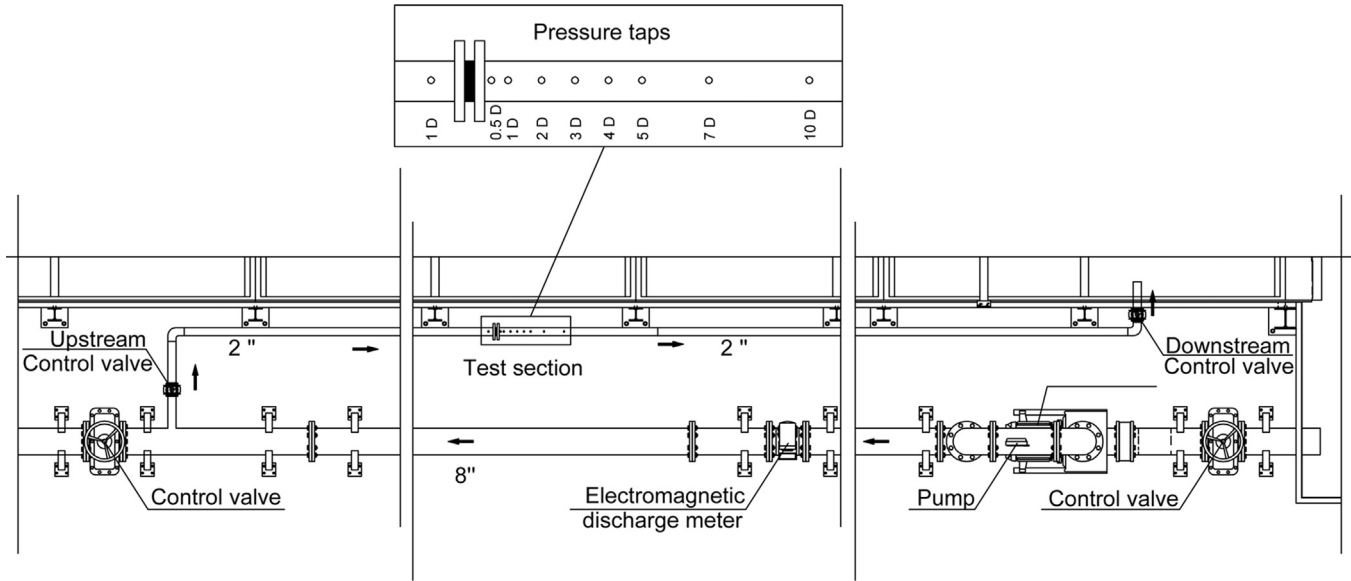
Fig. 3. Sketch of the test rig at the hydraulic laboratory of Politecnico di Bari University.

but other measurement taps were placed at $0.5D$, $1D$, $2D$, $3D$, $4D$, $5D$, $7D$ downstream the device. Discharge measurements were performed with an electromagnetic flowmeter, placed on the 203 mm pipe.

The tests were performed considering a fixed pressure at the downstream reference section, and gradually increasing the upstream pressure, thus increasing the discharge and consequently the Reynolds number.

Cavitation was detected from acceleration measurements, according to the ISA standard [38]. To this purpose a Brüel&Kjær 4397 accelerometer with sensitivity of 1.02 mV/(m/s^2) and resolution of 0.025 m/s^{2}was used; in addition, in order to further improve the reliability of the results, acceleration was also measured using a Brüel&Kjær 2513 portable integrating vibration meter. At the same time, Sound Pressure Level (SPL) was recorded by means of a Brüel&Kjær4191 Falcon Range microphone.

The experiments carried out by Politecnico di Milano University were performed in a pilot plant located at Pibiviesse S.r.l, Nerviano, Italy. The rig, shown in Fig. 4, consists of 254 mm (10 in) and 305 mm (12 in) steel pipes, supplied by a pump able to guarantee pressures up to 10 bar at the reference section upstream the plate. The testing line, which has a nominal diameter of 76.2 mm (3 in) and an actual diameter of 77.9 mm, is 7.42 m long, corresponding to about 95 pipe diameters. The plate is placed 4.40 m ($\approx 55D$) downstream the testing line inlet. Control valves placed upstream and downstream the test area allow setting the proper fluid-dynamic conditions in each experimental test. Pressure was mea-sured with two absolute pressure transducers PTX 7500, whose range is between 0–10 bar and the band pass filter varies from 0 to 1000 Hz. These devices were placed in reference sections located $2D$ upstream and $6D$ downstream the device, according to the ISA standard [38]. Other measurement points were placed $1D$ upstream and $1D,2D,3D,4D,5D,6D,$and $7D$ downstream the plate. Flow rate was measured by a 254 mm (10 in) electromagnetic flow meter, placed upstream the testing line. During the tests, the water temperature was measured in order to monitor values of density, viscosity, and vapor pressure of the fluid. The tests have been performed maintaining constant pressure at the upstream reference section P_1 and decreasing the downstream pressure P_2 in order to increase the discharge and consequently the Reynolds number. A single PCB Piezotronics 352A60 accelerometer was used to measure the pipe wall acceleration. The instrument has a sensitivity

of 1.02 mV/(m/s^2), range equal to ± 4905 m/s^2 and broadband resolution equal to 0.02 m/s^2. A sound level meter with sensitivity of 50 mV/Pa was used to measure the sound pressure level to further characterize the cavitation regime and confirm the relia-bility of the estimation of the incipient cavitation number.

In both campaigns, the plates were tested over a wide range of flow rates and consequently, of hole Reynolds numbers Re_h. For each Re_h, the pressures across the device and the acceleration level were recorded, and the corresponding values of C_d and σ calculated. The incipient cavitation number σ_i was estimated from the vibration data using the ISA standard [38] procedure; particularly, we plotted the natural logarithm of the acceleration versus the natural logarithm of σ, as shown in Fig. 5(a) for a typical plate, and performed a regression analysis ($y=mx+b$) for the two linear sections of data evident in the figure. The incipient cavitation number was the point of intersection of the two lines. For the same flow conditions depicted in Fig. 5(a), the values of C_d are plotted against Re_h in Fig. 5(b). As observed also by Maynes et al.[18], when $\sigma \approx \sigma_i$ the discharge coefficient C_d does not depend upon Re_h. Therefore, in order to increase the reliability of our data, the discharge coefficient of each plate was evaluated as the average of the values within the self-similarity region with respect to Re_h, identified in Fig. 5(b). Moreover, the estimates of C_d and σ_i referring to different values of operating pressure were averaged to take advantage of the absence of pressure scale effects on these two parameters, as already known [1,2,17,18,21,23,33] and further discussed in the "Results and discussion" section. The estimated value of σ_i was then checked with reference to measurements of sound pressure level which, according to the ISA standard [38], plays the same role as acceleration in the determination of σ_i.

Finally, the average total uncertainties on C_d and σ_i are 2.5% and 9.0% for the plates tested by the research group of Politecnico di Bari University using the rig sketched in Fig. 3, and 3.2% and 10.2%for the plates tested by the research group of Politecnico di Milano University in the rig represented in Fig. 4. Further details on the uncertainty analysis are provided in Appendix A.

Several plates with either single or multiple holes were tested in the two campaigns. The geometrical characteristics of the devices, expressed in terms of both dimensional quantities and dimensionless parameters, are summarized in Table 1. All plates have non-chamfered holes and the entry and exit hole edges are sharp with no measurable radius of curvature. No discernible changes occurred in
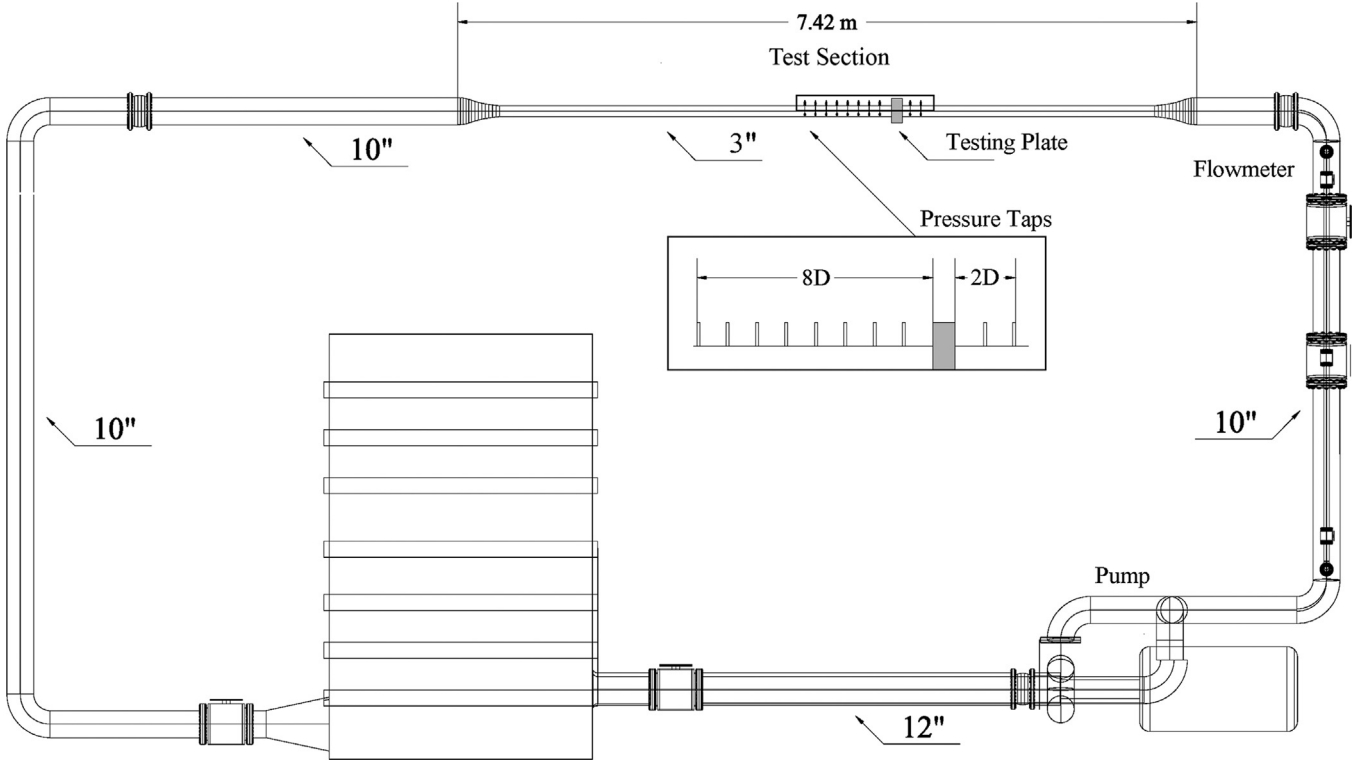
Fig. 4. Sketch of the test rig at Pibiviesse Srl (experiments of Politecnico di Milano University).
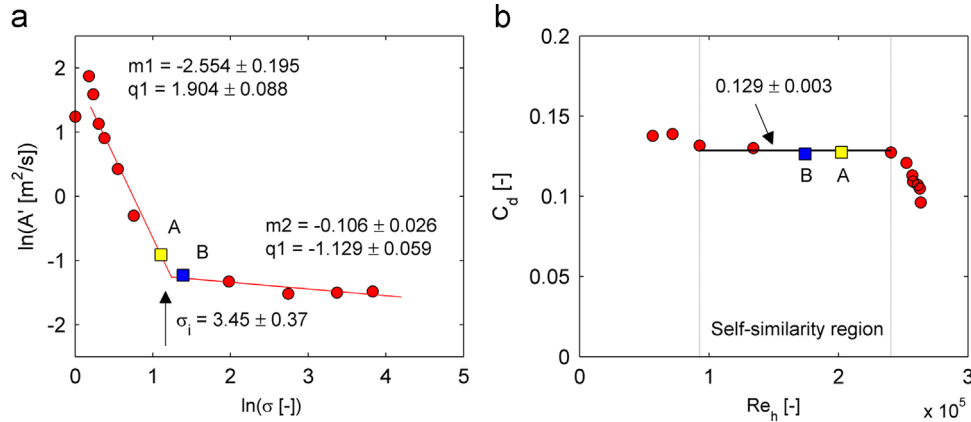

Fig. 5. Data referring to plate M3 in Table 1 with upstream pressure P_1=5.5 bar: (a) trend of $\ln(A')$ versus $\ln(\sigma)$. The incipient cavitation number σ_i is the abscissa of the intersection point of the two linear regressions; (b) trend of C_d versus Re_h. The highlighted corresponding points A and B help in verifying that, when $\sigma \approx \sigma_i$, C_d does not depend upon Re_h.

the shape of the holes during testing. Single-hole orifices are defined in terms of equivalent diameter ratio β and relative thickness t/d_h, which vary in the ranges $0.17 \leq \beta \leq 0.60$ and $0.11 \leq t/d_h \leq 1.00$, respectively. The equivalent diameter ratio β was varied by changing the hole size d_h for a fixed pipe diameter D. For each β, different values of t/d_h are attained by varying the hole thickness t. The multi-hole orifices have multiple equally-sized circular holes, and are thus completely defined in terms of β (from 0.18 to 0.60), t/d_h (from 0.19 to 4.40), number of holes (from 4 to 15), and distribution of the holes. The plates B8 to B31, tested in the rig sketched in Fig. 3, were obtained from slabs with three different thicknesses t (3, 5, 11 mm), subjected to n_h=4, 9, 13, 15 perforations of diameters d_h ranging from 2.5 to 16 mm. The combinations of t, n_h, and d_h were chosen in such a way as to allow one-at-a-time variations of β, t/d_h, and n_h. The plates M5 and M6, tested in the rig of Fig. 4, are characterized by the same values of β=0.40 and n_h=13 and two different values of

t/d_h=1, 1.40, obtained by changing the hole thickness t. The machining tolerances are reported in Appendix A.

3. Results and discussion

This section is divided in two parts. In the former, the dependence of the incipient cavitation number upon significant geometrical parameters (namely the equivalent diameter ratio β, the relative thickness t/d_h, and the number of holes n_h) is discussed. In the latter, a tool for performing effective estimation of the incipient cavitation number is provided, targeting the needs of accuracy and wide applicability. For these purposes, our experimental data were combined with those collected by previous researchers referring to single- [1,21,38] or multi-hole orifices [18] with non-chamfered hole edges. This allowed creating a large database of measurement including 1)

Table 1
Geometrical features of all the tested plates (B-plates: tested in the rig sketched in Fig. 3; M-plates: tested in the rig sketched in Fig. 4).

Plate ID	D [mm]	d_h [mm]	t [mm]	β [-]	t/d_h [-]	n_h [-]	Distribution of the holes
B1	53	9	3	0.17	0.33	1	
B2		9	5	0.17	0.56		
B3		16	5	0.30	0.31		
B4		16	11	0.30	0.69		
B5		26	5	0.49	0.19		
B6		32	5	0.60	0.16		
B7		32	11	0.60	0.34		
B8	53	5	3	0.19	0.60	4	
B9		5	11	0.19	2.20		
B10		8	5	0.30	0.63		
B11		8	11	0.30	1.38		
B12		13	3	0.49	0.23		
B13		13	5	0.49	0.38		
B14		16	3	0.60	0.19		
B15		16	11	0.60	0.69		
B16	53	5	3	0.28	0.6	9	
B17		5	5	0.28	1.00		
B18		5.5	11	0.31	2.00		
B19		9	3	0.51	0.33		
B20		8	5	0.45	0.63		
B21		8	11	0.45	1.38		
B22	53	4.5	3	0.31	0.67	13	
B23		4	5	0.27	1.25		
B24		4	11	0.27	2.75		
B25		7	3	0.48	0.43		
B26		7	11	0.48	1.57		
B27	53	2.5	3	0.18	1.20	15	
B28		3	5	0.23	1.67		
B29		2.5	11	0.18	4.40		
B30		8	3	0.58	0.38		
B31		8	5	0.58	0.63		
M1	77.9	30.5	7.3	0.39	0.24	1	
M2		30.5	13.7	0.39	0.45		
M3		30.5	22.3	0.39	0.73		
M4		30.5	30.5	0.39	1.00		
M5	77.9	8.4	8.4	0.40	1.00	13	
M6		8.4	11.8	0.40	1.40		

Fig. 6. Trend of $\ln(A')$ versus $\ln(\sigma)$ for plate M3 in Table 1. The data refer to two different values of test pressure P_1. The estimated incipient cavitation number is identified together with its uncertainty.

Fig. 7. Trend of σ_i/SSE as a function of β for all the data available.

single-hole orifices with D between 27 mm and 597 mm, d_h between 9 and 477 mm, and t up to 38 mm, spanning the following range of dimensionless variables: β between 0.17 and 0.88; and t/d_h up to 1; 2) multi-hole orifices with D between 53 and 100 mm, n_h between 4 and 1793, d_h between 2 and 25 mm, t between 3 and 12 mm, spanning the following range of dimensionless variables: β between 0.18 and 0.66; and t/d_h between 0.19 and 4.40. In order to account for the already mentioned size-scale effects, the values of σ_i of the different plates were made comparable by applying Eq. (12) (D_{ref} was 0.076 m). Data from literature will be denoted by the reference where they come from. It is worth mentioning that only the experiments of Maynes et al. [18], who reported a detailed uncer-tainty analysis, allowed us to take into account the uncertainty of the literature data included in the database. In particular, they declared an average total uncertainty of $\pm4.1\%$ in their Eu values and an uncertainty of 10.4% for σ_i. These values appear comparable with those estimated for both our data series.

The effect of the pressure on the estimate of σ_i was first addressed. It has already been remarked in the "Introduction" that several authors argued for the absence of pressure scale effects associated with the incipient cavitation of perforated plates [1,21,23,33]. Our experiments, performed at different plant pressures, confirmed this behavior. As an example, Fig. 6 shows the plot of $\ln(A')$ versus $\ln(\sigma)$ for the plate referred to as M3 in Table 1. The experiments were carried
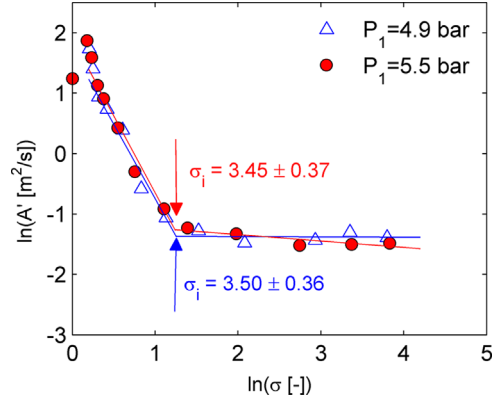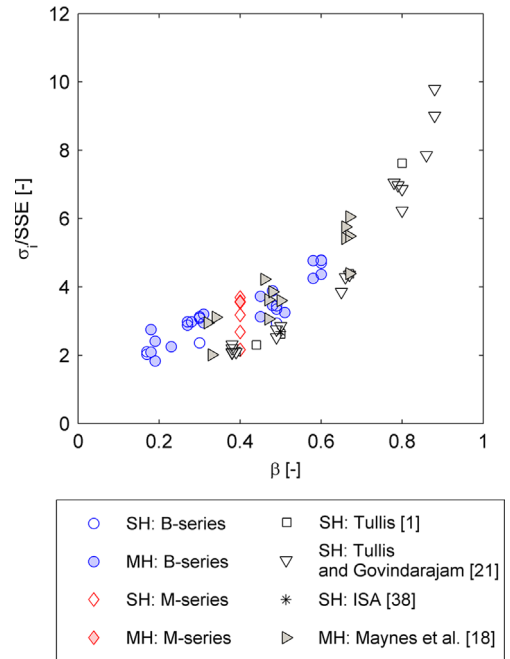
out for two different values of upstream test pressure, equal to 4.9 and 5.5 bar, respectively. The substantial coincidence between the estimates of σ_i suggests the absence of any significant pressure-scale effect. Hereafter we will refer to σ_i as the average among the values obtained at different test pressures. We will now investigate the dependence of σ_i upon the geometrical characteristics of the devices.

Fig. 7 shows the trend of σ_i/SSE as a function of the equivalent diameter ratio β for all items of the database. The plot highlights the strong influence of β on σ_i/SSE and, particularly, that σ_i/SSE increases as β increases, extending to a wider range of plates the findings of previous works [1,2,15,18,20,21,23]. The considerable data scattering for a given β indicates that other geometrical parameters such as t/d_h and n_h have a significant influence. However, Fig. 7 does not allow establishing the role played by these variables and, particularly, the difference between the single and multi-holed data.

The effect of the relative thickness is then analyzed in detail, being well known that t/d_h influences the flow regime through the plate. For low values of t/d_h a fully-separated flow regime takes place, that is, the jet remains separated from the orifice wall;
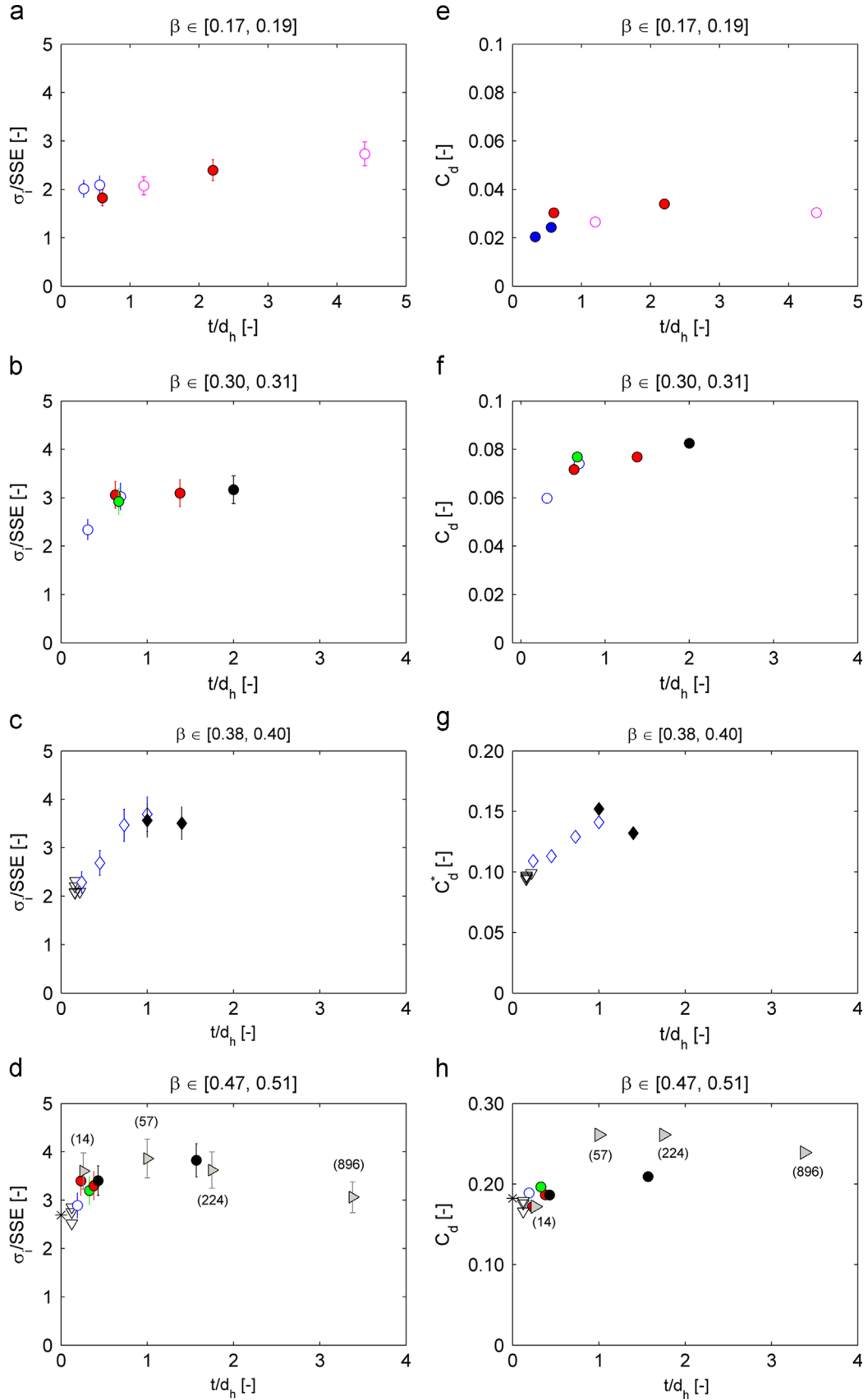
Fig. 8. Trend of σ_i/SSE (left-hand side) and C_d (right-hand side) as a function of t/d_h for small ranges of β, indicated in the title of the plots. The effect of n_h is highlighted too. Legend: ○: B-series, single-hole; ●: B-series, multi-hole with $n_h=4$; ●: B-series, multi-hole with $n_h=9$; ●: B-series, multi-hole with $n_h=13$; ○: B-series, multi-hole with $n_h=15$; ◇: M-series, single-hole; ◆: M-series, multi-hole with $n_h=13$; ▽: Tullis and Govindarajan [21], single-hole; ✳: ISA [38] sharp-edge single-hole; ▷Maynes et al. [18], multi-hole with the number of holes indicated between brackets. When possible, error bars indicating the uncertainty in σ_i/SSE are drawn. The uncertainty in C_d is too small to be visibile.

conversely, when the t/d_h ratio is high the flow is fully-reattached, that is, the jet reattaches into the inner wall to the orifice hole and then expands to the pipe. The threshold value of t/d_h between the two regimes is not well defined and typically varies between 0.5 and 1 [18,40,41].

Fig. 8(a-d) show the trend of σ_i/SSE as a function of t/d_h for different small ranges of β. The data depicted in the plots refer to either single- or multi-hole orifices. Error bars indicating the uncertainty in the σ_i/SSE values are reported for our data and those of Maynes et al. [18], since this information is not available for the other experiments. It can be observed that σ_i/SSE increases with t/d_h when the jets do not reattach to the inner wall of the holes, that is, for t/d_h lower than 0.5–1. The effect of t/d_h on the incipient cavitation number is instead not univocal for $t/d_h > 1$, where fully-reattached flow occurs. The data showed a slightly increasing trend of σ_i/SSE with t/d_h for small values of β, whilst a decreasing trend was identified by Maynes et al. [18] for $\beta \geq 0.5$. The influence of n_h upon σ_i/SSE for β and t/d_h being the same has not been completely clarified, but apparently it seems minor if compared with that of the parameters already discussed. Fig. 8(e-h) are analogous of Fig. 8(a-d) and show the discharge coefficient C_d on the vertical axes. There appears correspondence between the two columns of Fig. 6, since the trends of σ_i/SSE and C_d are very similar when plotted against t/d_h. This result, observed also by Maynes et al. [18] in terms of the Euler number and limited to their multi-hole data, gives strength to the hypothesis of a link between cavitation number and dissipation characteristics, and suggests that the discharge coefficient allows condensing into a single parameter the combined effects of β, t/d_h, n_h and, possibly, the distribution of the holes on the incipient cavitation number. This will be further discussed in the following.

As already stated, the objective of the second part of this article is to provide a correlation with the widest possible applicability for providing reliable estimation of the incipient cavitation number, trying to take into account the effects of all the relevant para-meters previously identified. In order to achieve this goal we started from the analysis of the models available in the literature.

The physically-based models of Nurick [24] (Eq. (6)) and Sanchez et al. [31] (Eq. (8)) were considered first. The former model was developed for single-hole orifices, and therefore we tested its predictive capacity when it is applied to these devices. Fig. 9 shows the parity plot "predicted σ_i/SSE" versus "measured σ_i/SSE" for the model of Nurick [24], in which the contraction coefficient is evaluated by means of Eq. (7). As expected, the model of Nurick [24] consistently underestimates the incipient cavitation number, owing to the assumption of putting the pressure at the vena contracta section equal to the vapor pressure. Due to its poor performance even for single-hole orifices, this model was not helpful for developing a new correlation of wider applicability.

The model of Sanchez et al. [31] (Eq. (8)) removes the hypothesis that the pressure at the vena contracta section equals the vapor one by accounting for the effect of the fluctuating pressure by means of an empirically determined coefficient c'. The model relies on a physical basis and has been derived for single-hole orifices. Nevertheless, it was tested against the whole database since the authors themselves mention the possibility of applying Eq. (8) to other devices. The parity plot in Fig. 10 was obtained by evaluating c' as $2.9D[m]^{0.5}$, as proposed by Sanchez et al. [31] by best-fitting some single-hole orifice data from Tullis [22]. Once again, the contraction coefficient is evaluated by means of Eq. (7). In comparing the predictions with the experimental data, the SSE factor (Eq. (12)) was not applied since the amplitude of the pressure fluctuations is related to the pipe diameter. The consider-able dispersion of the points in Fig. 10 indicates that, in the present form, the predictive capacity of Eq. (8) is rather poor. Currently the main limitation of the model of Sanchez et al. [31] resides in its dependence upon a parameter whose determination is still
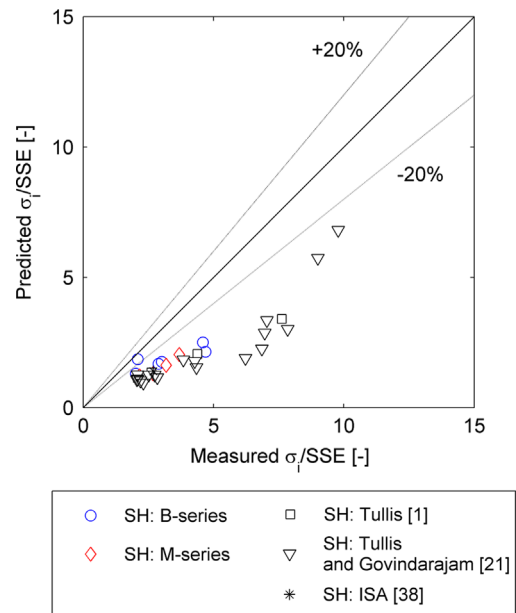

Fig. 9. Parity plot "predicted σ_i/SSE" versus "measured σ_i/SSE" according to the model of Nurick [24] (Eq. (6)). Only the data referring to single-hole orifices have been considered.
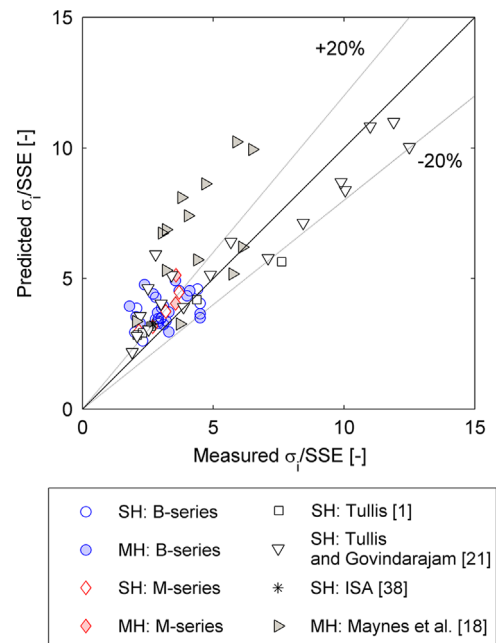

Fig. 10. Parity plot "predicted σ_i" versus "measured σ_i" according to the model of Sanchez et al. [31] (Eq. (8)). The model has been tested against the whole database.

uncertain and call for future research, as observed by these researchers themselves.

As a result of the above-reported considerations we turned our attention on the three available empirical correlations which, as already noticed, differ in the set of related parameters: the model of Kuroda et al. [25] (Eq. (9)) relates σ_i to β, the model of Tullis [2] (Eq. (10)) relates σ_i to C_d, and, in closing, the model of Maynes et al. [18] (Eq. (11)) relates $(\sigma_i-1)/(1-0.1t/d_h)$ to C_d. Our goal was primarily to establish the extent to which each set of indepen-dent/dependent variables allows explaining the behavior of the whole dataset at our disposal. Afterwards, based on these results a new correlation was proposed.
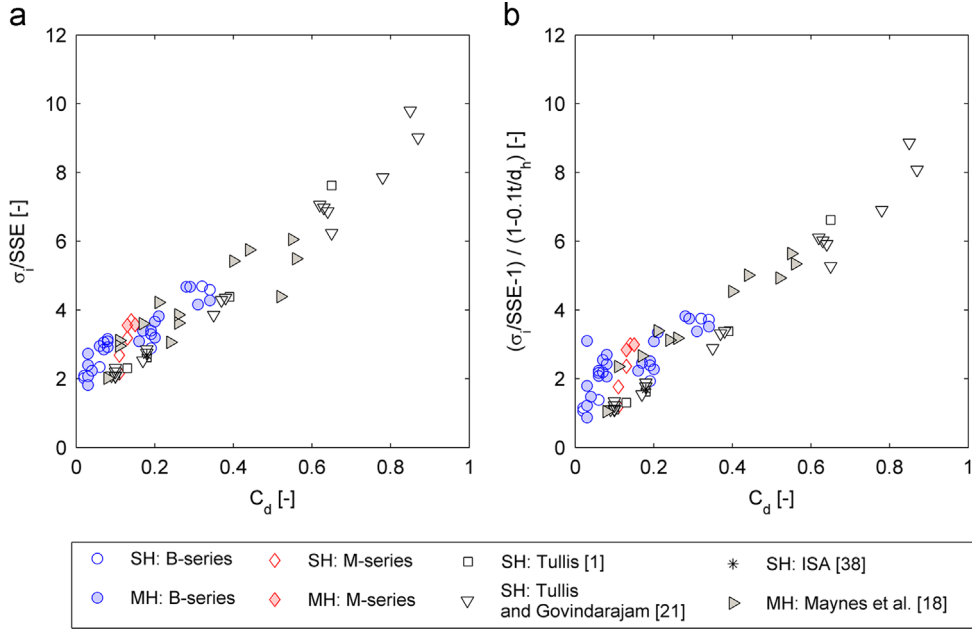
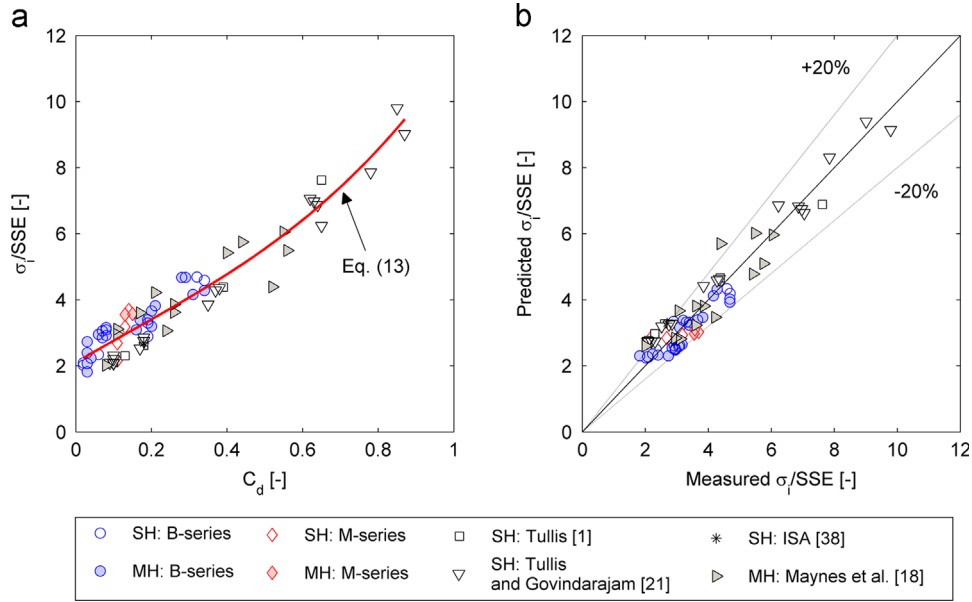**Fig. 11.** All values of the discharge coefficient plotted against: (a) σ_i/SSE (b) $(\sigma_i/SSE\text{-}1)/(1\text{-}0.1t/d_h)$.

Fig. 12. (a) Trend of σ_i/SSE against C_d: comparison between experimental data and Eq. (13). (b) Parity plot "predicted σ_i" versus "measured σ_i". The whole database has been considered.

It has already been observed (Fig. 7) that, for a given β, a significant variation in the σ_i values occurs due to the influence of other geometrical parameters such as mainly t/d_h and n_h. There-fore, a correlation in which β is the only independent variable, like that of Kuroda et al. [25] (Eq. (9)), is not expected to yield a completely accurate prediction of the incipient cavitation number. The model of Tullis [2] (Eq. (10)) uses the discharge coefficient C_d as independent variable. Tullis derived his correlation by fitting his own experimental data regarding single-hole orifices with $t/d_h \approx 0$, in which β is the only relevant geometrical parameter. We have already remarked that, in case of perforated plates, C_d depends on several geometrical parameters [17,18] and therefore its use as independent variable can represent an efficient way to account for their combined effect on the incipient cavitation

number. In Fig. 11(a) the incipient cavitation number is plotted against the discharge coefficient for the whole database. The relatively low data scattering (attributable to the uncertainty in the experimental estimates and, possibly, the influence of other parameters affecting the experiments) gives strength to the hypothesis of a link between cavitation inception and dissipation characteristics of the device, and suggests that a correlation in which C_d is the independent variable may satisfy the accuracy and wide applicability requirements of the new correlation. Apparently no clear difference in the behavior of single and multi-hole data can be identified.

Maynes et al. [18] used C_d as independent variable and $(\sigma_i - 1)/(1 - 0.1t/d_h)$ as dependent one in order to limit the variability of the data attributed to the effect of t/d_h. They referred to their own

multi-holed data and few single- and multi-hole measurements available in the literature, covering a wide range of parameters (particularly, between 0.076 and 0.0648 in terms of C_d). In order to explore the opportunity of making such a change of variables, we plotted the discharge coefficient C_d versus $(\sigma_i/SSE\text{-}1)/(1–0.1t/d_h)$ for all the available data. The results, reported in Fig. 11(b) reveal that replacing σ_i/SSE with $(\sigma_i/SSE\text{-}1)/(1–0.1t/d_h)$ has the effect of reducing the scattering of the measurements of Maynes et al. [18] but, at the same time, increases the variability of the other data especially below the lower bound of the range of C_d considered by the authors.

Based on the proposed analysis it can be concluded that a formula relating σ_i/SSE to C_d provides the best explanation of the data and, therefore, can be used to obtain reliable estimations of the incipient cavitation number of perforated plates. Like Tullis [2], we propose a third-order polynomial expression obtained by fitting all the data available:

$$\frac{\sigma_i}{SSE} = 2.10 + 6.75 \cdot C_d - 1.99 \cdot C_d^2 + 4.55 \cdot C_d^3 \qquad (13)$$

The results are summarized in Fig. 12 that clearly shows the good predictive capacity of Eq. (13), which is applicable to single- and multi-hole orifices with diameter ratios β between 0.17 and 0.88, relative thickness t/d_h up to 4.40, and number of holes n_h up to 1793. The discharge coefficient C_d varies between 0.02 and 0.87.

4. Conclusion

In this article, the incipient cavitation number of perforated plates was investigated. The research is based upon a large experimental campaign, carried out by two research groups from Politecnico di Bari University and Politecnico di Milano University. After being checked for consistency and made comparable, relevant data from literature were added, so allowing reliable assessment of the dependence of the incipient cavitation number on the most significant geometrical and flow parameters. The whole database includes experimental data regarding both single- and multi-hole orifices (for a total of 75 devices) with equivalent diameter ratio β between 0.17 to 0.88, relative thickness t/d_h up to 4.40, and number of holes up to 1793.

The analysis confirms that the incipient cavitation number is strongly affected by β. In particular, a reduction of the porosity of the plate, that is, lower β, results in a delayed onset of cavitation and, therefore, lower incipient cavitation number (Fig. 7). The relative thickness t/d_h plays an important role too, being directly connected to the flow configuration within the holes. The incipient cavitation number increases with t/d_h when fully-separated flow occurs, and reaches the maximum value when the transition to fully-reattached flow takes place. Depending on β, the incipient cavitation number may either increase or decrease with t/d_h when fully-reattached flow occurs (Fig. 8). Even if the data available did not allow complete clarification of the role played by the number of holes, this parameter seems to have a minor influence com-pared to β and t/d_h.

Starting from the analysis of the literature formulas developed for the estimation of the incipient cavitation number σ_i and applicable to a smaller range of flow conditions, it is found that, for all the items of the database, the combined effects of β, t/d_h and, possibly, number and distribution of the holes on the incipient cavitation number σ_i seem to be fairly well explained by the discharge coefficient C_d (Fig. 11(a)). Therefore, it is proposed a new correlation relating σ_i to C_d which provides reliable predic-tion of the incipient cavitation number of perforated plates (Fig. 12) and it is applicable to a very wide range of devices (either single- or multi-holed).

Appendix A. Uncertainty analysis

Our data are subjected to several uncertainties which, in turn, depend on those of the measurements of P_1, P_2, T, t, d_h, and V, and A'. The perforation hole diameter and plate thickness uncertainty were ± 0.05 mm, as declared by the manufacturer. In compliance with this machining tolerance, the edges of the holes can be considered sharp. The uncertainty on P_1 and P_2, depending on the used transducers, was found lower than about 2% in both experimental rigs. The uncertainty on the pipe bulk-mean velocity V was considered equal to 0.25% and 0.2% of the full scale for the experiments performed in the rigs sketched in Figs. 3 and 4, respectively, as declared by the manufacturers of the used flow-meters. The uncertainty of the acceleration A' is quantified by the broadband resolution of the accelerometer, and the reliability of the acceleration measurements was further guaranteed by the fact that the specifications of the instrumentation meet the require-ments of the ISA standard [38]. The uncertainties in the measure-ments acquired are reported in Table A1 for the two sets of experiments.

The estimate of the uncertainty in β, t/d_h, ρ, P_V, C_d, and σ, reported in Table A2, was provided in respect to the International Organization of Standardization-GUM [42] by applying the error combination law. The water density ρ was not measured directly, but inferred from the temperature using the tabular values reported in a standard chemical textbook [43]. In the same way, the ITS-90 formulations [44] were employed to quantify the vapor pressure P_V from temperature measurements. The uncertainty of the variable C_d in Table A2 represents the error associated to each point in the C_d versus Re_h plots (see Fig. 5(b)). However, the actual uncertainty on the discharge coefficient on each plate, which was evaluated as the average of the data within the self-similarity region with respect to Re_h, was around 2.5% and 3.2% for the experiments carried out in the rigs sketched in Figs. 3 and 4, respectively.

The procedure followed for the estimation of the incipient cavitation number σ_i has been described in detail in the "Test rigs and experimental procedure" Section. Substantially, we applied the interpolation-based method described in the ISA standard [38] and then averaged the estimates referring to different values of operating pressure to take advantage of the absence of pressure scale effects [1,2,17,18,21,23,33]. The uncertainty on σ_i accounts for the propagation of error from the measurements performed, the regression analysis employed, and the averaging over the different operating pressures. For the experiments carried out by the research group of Politecnico di Bari University, the average total

Table A1
Uncertainty in the measurements acquired (B-series: tests performed by in the rig sketched in Fig. 3; M-series: tests performed in the rig sketched in Fig. 4).

Uncertainty	B-series	M-series
$u(t)$	± 0.05 mm	± 0.05 mm
$u(d_h)$	± 0.05 mm	± 0.05 mm
$\varepsilon(P_1)$	$\pm 1.5\%$	$\pm 0.5\%$
$\varepsilon(P_2)$	$\pm 1.5\%$	$\pm 1.8\%$
$u(T)$	± 0.5 °C	± 0.5 °C
$\varepsilon(V)$	$\pm 0.25\%$	$\pm 0.2\%$
$u(A')$	± 0.025 m/s^2	± 0.02 m/s^2

Table A2
Uncertainties determined by applying the error combination law (B-series: tests performed by in the rig sketched in Fig. 3; M-series: tests performed in the rig sketched in Fig. 4).

Uncertainty	B-series	M-series
$\varepsilon(\beta)$	$\pm 0.87\%$	$\pm 0.41\%$
$\varepsilon(t/d_h)$	$\pm 1.4\%$	$\pm 0.5\%$
$u(\rho)$	$\pm 0.01\%$	$\pm 0.01\%$
$\varepsilon(P_V)$	$\pm 3\%$	$\pm 3\%$
$\varepsilon(C_d)$	$\pm 1.3\%$	$\pm 2.1\%$
$\varepsilon(\sigma)$	$\pm 5.0\%$	$\pm 4.5\%$

uncertainty on σ_i was 9.0%, with a maximum and minimum uncertainty of 13.0% and 6.0%, respectively. As far as the experiments of the research group of Politecnico di Milano University are concerned, $\varepsilon(\sigma_i)$ varied from 7.1% to 13.1%, with an average value of 10.2%.

References

[1] Tullis JP. Hydraulics of pipelines. Pumps, valves, cavitation, transients. New York, USA: John Wiley & Sons; 1989.
[2] Tullis JP. Cavitation guide for control valves. US Nuclear Regulatory Commission NUREG/CR-6031 (April 1993), Washington, DC.
[3] Laws EM, Ouazzane AK. A further investigation into flow conditioner design yielding compact installations for orifice plate flow metering. Flow Meas Instrum 1995;8(2):61–76.
[4] Schulter T, Merzkirch W. PIV measurements of the time-averaged flow velocity downstream of flow conditioners in a pipeline. Flow Meas Instrum 1996;7(3-4):173–9.
[5] Morrison GL, Hall KR, Holste JC, Ihfe L, Gaharan C, DeOtte Jr. RE. Flow development downstream of a standard tube bundle and three different porous plate flow conditioners. Flow Meas Instrum 1997;8(2):61–76.
[6] Xiong W, Kalkuhler K, Merzkirch W. Velocity and turbulence measurements downstream of flow conditioners. Flow Meas Instrum 2003;14(6):249–60.
[7] Liu R, Ting DSK. Turbulent flow downstream of a perforated plate: sharp-edged orifice versus finite-thickness holes. ASME J Fluid Eng 2007;129 (9):1164–71.
[8] Jones PD, Van Winkle M. Effect of plate thickness and system properties. Ind Eng Chem 1957;49(2):232–8.
[9] Kolodzie Jr. PA, Van Winkle M. Discharge coefficients through perforated plates. AIChE J 1957;3(3):305–12.
[10] Gan G, Riffat SB. Pressure loss characteristics of orifice and perforated plates. Exp Therm Fluid Sci 1997;14(6):160–5.
[11] Weber LJ, Cherian MP, Allen ME, Muste M. Headloss characteristics for perforated plates and flat bar screens. Technical Report. Iowa City (IA), USA: Iowa Institute of Hydraulic Engineering, College of Engineering, University of Iowa; 2000 Mar. Report No.: 411.
[12] Malavasi S, Messa GV, Macchi S. The pressure drop coefficient through sharp-edged perforated plates. Atti del XXXII Convegno Nazionale di Idraulica e Costruzioni Idrauliche IDRA2010; 2010 September 14–17, Università degli studi di Palermo, Palermo, Italy (on CD-ROM).
[13] Zhao T, Zhang J, Ma L. A general structural design methodology for multi-hole orifices and its experimental application. J Mech Sci Tech 2011;25(9):2237–46.
[14] Fratino U, Pagano A, Malavasi S, Messa GV. Pressure drop and recovery across sharp-edged multi-hole orifices. Proceedings of the second IAHR conference; 2012 June 27–29; Technische Universität Munchen, Munich, Germany (on USB-key).
[15] Holt GJ, Maynes D, Blotter J. Cavitation at sharp edge multi-hole baffle plates. Proceedings of the ASME 2011 international mechanical engineering congress & exposition IMECE2011; 2011 November 11–17; Denver, CO USA.
[16] Pagano A, Messa GV, Malavasi S, Fratino U. Definizione sperimentale dell'efficienza dissipativa di diaframmi a foro multiplo con geometria variabile (Experimental characterization of energy dissipations through multi-hole orifices with different geometry, in Italian). Atti del XXXIII Convegno Nazionale di Idraulica e Costruzioni Idrauliche IDRA2012; 2012 September 10–15, Brescia, Italy (on CD-ROM).
[17] Malavasi S, Messa GV, Fratino U, Pagano A. On the pressure losses through perforated plates. Flow Meas Instrum 2012;28:57–66.
[18] Maynes D, Holt GJ, Blotter J. Cavitation inception and head loss due to liquid flow through perforated plates of varying thickness. ASME J Fluid Eng 2013;135:131302.
[19] Numachi F, Yamabe M, Oba R. Cavitation effect on the discharge coefficient of the sharp-edged orifice plate. J Fluid Eng. 1960;82(1):1–6.
[20] Govindarajan R. Cavitation size scale effect. (Ph.D. thesis].). Fort Collins, CO USA: Colorado State University; 1972.
[21] Tullis JP, Govindarajan R. Cavitation and scale effects for orifices. J Hydr Div ASCE 1973;HY3:417–30.
[22] Tullis JP. Cavitation size scale effects for valves. Inf Sys 1973;99(HY7):1109–28.
[23] Ball JW, Tullis JP, Stripling T. Predicting cavitation in sudden enlargements. J Hydr Div ASCE 1975;101(7):857–70.
[24] Nurick WH. Orifice Cavitation and Its effect on spray mixing. ASME J Fluid Eng 1976;98(4):681–7.
[25] Kuroda M, Fukuda T, Cho T. Hydraulic experiments on pressure dissipation with orifices in conduit. Trans Jpn Soc Irrigat Drain Reclamat Eng 1978;78:57–64.
[26] Bistafa SR, Lauchle GC, Reethof G. Noise generated by cavitation in orifice plates. ASME J Fluid Eng 1989;111(3):278–89.
[27] Kim BC, Pak BC, Cho NH, Chi DS, Choi HM, Choi YM, et al. Effects of cavitation and plate thickness on small diameter ratio orifice meters. Flow Meas Instrum 1997;8(2):85–92.
[28] Ramamurthi K, Nandakumar K. Characteristics of flow through small sharp-edged cylindrical orifices. Flow Meas Instrum 1999;10(3):133–43.
[29] Zhang QY, Chai BQ. Hydraulic characteristics of multistage orifice tunnels. J Hydraul Eng 2001;127::663–8.
[30] Bikai Z, Yan H, Tiehua Z, Zhuangyun L. Experimental investigation of the flow characteristics of small orifices and valves in water hydraulics. Proc Inst Mech Eng Part E 2002;216(4):235–45.
[31] Sanchez R, Juana L, Laguna FV, Rodriguez-Sinobas L. Estimation of cavitation limits from local head loss coefficient. ASME J Fluid Eng 2008;130:101302.
[32] Malavasi S, Messa GV. Dissipation and cavitation characteristics of single-hole orifices. ASME J Fluid Eng 2011;133:051302.
[33] Fratino U. Hydraulic and cavitation characteristics of multihole orifices. In: Proceedings of the hydraulic machinery and system 20th IAHR symposium; 2000 August 6–9, Charlotte, NC USA (on CD-ROM).
[34] Takahashi K, Matsuda H, Miyamoto H. Cavitation characteristics of restriction orifice (experiment for shock ressure distribution by cavitation on restriction orifices and occurrence of cavitation at multiperforated orifices due to interference of butterfly valve). In: Proceedings of the fourth international symposium on cavitation CAV2001; 2001 June 20–23, California Institute of Technology, Pasadena, CA USA.
[35] Testud P, Massou P, Hirschberg A, Auregan Y. Noise generated by cavitating single-hole and multi-hole orifices in a water pipe. J Fluid Struct 2007;23 (2):163–89.
[36] Malavasi S, Macchi S, Mereghetti E. Cavitation and dissipation efficiency of multihole orifices. In: Prague CZ, Prague I, Zolotarev,, Horacek J, editors. Proceedings of the nineth international conference on flow-induced vibrations FIV2008. 2008 Jun 30–Jul 3. Institute of Thermomechanics Academy of Sciences of the Czech Republic; 2008. p. 581–6.
[37] Brennen CE. Cavitation and bubble dynamics. New York, USA: Oxford University Press; 1995.
[38] ISA Considerations for evaluating control valve cavitation, ISA-RP75.23-1995 (June 2, 1995).
[39] Rahmeyer WJ. Predicting and modeling cavitation damage: sudden enlargement. (Ph.D thesis]). Colorado State University: Fort Collins, CO USA; 1980.
[40] Ward-Smith AJ. Pressure losses in ducted flows. London, UK: Butterworths; 1971.
[41] Chisholm D. Two-phase flow in pipeline and heat exchangers. London, UK: George Godwin; 1983.
[42] Guide to the expression of uncertainty in measurements. ISO-GUM, Part 1–15; 1993.
[43] Weast RC, Astle MJ, Beyer WH. CRC handbook of chemistry and physics. Boca Raton, Florida: CRC Press; 1989.
[44] Hardy B. ITS-90 formulations for vapor pressure, frost point temperature, dew point temperature and enhancement factors in the range -100 to $100\,^\circ$C. In: Proceedings of the 3rd international symposium on humidity and moisture; National Physical Laboratory UK; 1998. p. 214–221.